Mixing enhancement by pulsating chaotic advection

Mojtaba Jarrahi, Cathy Castelain, Hassan Peerhossaini

MIXING ENHANCEMENT BY PULSATING CHAOTIC ADVECTION

Mojtaba Jarrahi[1,2], Cathy Castelain[1] and Hassan Peerhossaini[3*]

[1] Thermofluids, Complex Flows and Energy Group, Laboratoire de Thermocinétique, UMR CNRS 6607, Nantes University , La Chantrerie, BP 50609, F-44306, Nantes, France

[2] Univ. Paris-Sud, LIMSI-CNRS UPR 3251, BP 133, 91403 Orsay Cedex, France.

[3] Univ. Paris Diderot, Sorbonne Paris Cité, Institut des Energies de Demain-CNRS FRE 3597, Paris, France

[*]Corresponding author:

Phone: (33) 607 53 31 61

E-mail: hassan.peerhossaini@univ-paris-diderot.fr

Abstract

The purpose of this study is to investigate transverse mixing enhancement by superposition of periodic time dependence, in the form of pulsation, on a twisted pipe flow in which the fluid particles trajectories are spatially chaotic. The pulsation makes the secondary flow structure more complex, resulting in stronger velocity gradients that enhance stretching and folding, the main mechanisms of chaotic mixing. Here, the chaotic configuration is six alternating 90° curved pipes. The imposed pulsating conditions range as follows: steady Reynolds numbers $420 \leq Re_{st} \leq 1000$, velocity component ratios $1 \leq (\beta = U_{\max,osc}/U_{m,st}) \leq 4$ and frequency parameters $8.37 < (\alpha = r_0(\omega/\nu)^{0.5}) < 24.5$. The secondary velocity fields are measured by particle image velocimetry. The axial vorticity and transverse strain rate at the outlet of each curved pipe in pulsatile flow are compared with those of the steady flows. Analysis of these criteria for mixing assessment shows that $\beta \geq 2$ and $\alpha \leq 15$ are favorable pulsating conditions for transverse mixing enhancement. Moreover, in some pulsation conditions, the cell centres visit a zone in the flow cross-section that is much larger than in the steady case, implying that pulsation also contributes to mixing homogenization.

Keywords: Mixing, Pulsating flow, Chaotic mixer, Secondary flow, Dean flow, Lyne instability

1. Introduction

Mixing enhancement in laminar flows is significant in such industries as pharmacologicals, foods, polymer and chemicals. In these sectors, however, turbulent flows are rarely used despite their mixing advantages because the large stresses in a turbulent flow may affect the quality of the product (usually long, fragile molecular chains). In such situations mixing can be carried out only in laminar flows, and intensification of mixing in such flows requires new techniques.

Chaotic advection, introduced by Aref [1], analyzes the macroscopic transport of tracers in spatially chaotic trajectories generated by simple laminar velocity fields. It is the special geometry of the system that allows these chaotic trajectories to be produced. The chaotic nature of the streamlines in alternating Dean flow has the same cause: the geometrical perturbation of a steady Dean flow (flow in a curved pipe). This perturbation is introduced by successive changes in the orientation of the curvature plane. At each change in orientation, the centrifugal force is reoriented and thus the Dean cell positions are modified in such a way that cells are destroyed and reconstructed in a perpendicular plane. Since the Dean cells play the role of "agitators," their alternating displacement and reorientation contribute to better stirring and consequently better mixing. Moreover, the analysis of the residence time distribution has shown [2,3] that axial dispersion in the alternating Dean flow is more than 20% less than in a helicoidally coiled-pipe flow having the same number of bends. The decrease in axial dispersion, accompanied by an increase in transverse dispersion, is due to the generation of chaotic trajectories and contributes to mixing enhancement. Several studies have been carried out on mixing improvement and also heat-transfer enhancement in steady alternating Dean flows [4-8].

Much previous research on pulsating flow in curved pipes has been motivated by physiological applications [9-15]. Simon et al. [16] investigated the effects of pulsation on heat-transfer enhancement. In the present work, we are interested in the effects of pulsation on mixing improvement in alternating Dean flow. Timité et al. [17] demonstrated some of the potential of pulsating alternating Dean flow using laser-induced fluorescence (LIF) visualizations; although qualitative, these images revealed an important modification in the secondary flow structure due to the pulsation. Under certain pulsating conditions, the secondary flow becomes more complex, with the appearance of Lyne instability [18] or swirling structures. Moreover, Timité et al. [17] showed by a Lagrangian method that superposition of an oscillation on a steady alternating Dean flow reduces the non-stretching zones in the flow. This phenomenon was observed by following the tracer spreading at different bend outlets.

This work aims to characterize experimentally the secondary flow and transverse mixing in pulsating alternating Dean flow. The paper is organized as follows: section 2 describes the experimental setup and measurement techniques. The PIV measurements allow the detailed Eulerian analysis of the secondary flow presented in section 3. It has been shown that the complex structures reported in one bend of a chaotic configuration [19-21] persist in successive bends but in a more convoluted shape. Complexity of flow topology is important for mixing because it can provide stronger vorticity and strain rates and thus better stirring. In order to better understand the effects of pulsation on the secondary flow patterns and transverse mixing in alternating Dean flow, the steady state is studied first, and then the displacements of the cells and variations in mixing are analyzed for different pulsating

conditions. The pulsating conditions studied here range as follows: steady Reynolds numbers $420 \leq Re_{st} \leq 1000$, velocity component ratios $1 \leq (\beta = U_{max,osc}/U_{m,st}) \leq 4$ and frequency parameters $8.37 < (\alpha = r_0(\omega/\nu)0.5) < 24.5$. Concluding remarks, presented in section 4, discuss the effects of pulsation on mixing enhancement in alternating Dean flow.

2. Experimental setup and measurement techniques

The velocity field of the pulsating flow U_P can be expressed as

$$U_P(t) = U_{mS} + U_{\max,\sin} \sin(\omega t) \qquad (1)$$

where U_{mS} is the mean velocity of the steady flow and $U_{\max,\sin}$ is the velocity amplitude of the sinusoidal flow. If we define a dimensionless velocity component ratio as the ratio between these values:

$$\beta = \frac{U_{\max,\sin}}{U_{mS}} \qquad (2)$$

equation 1 can be written as

$$U_P(t) = U_{mS}\left(1 + \beta \sin(\omega t)\right) \qquad (3)$$

Another dimensionless parameter, the Womersley number, α, can be used to describe the angular velocity ω in equation 3. The Womersley number represents the inertial effects due to pulsating flow frequency in relation to viscous effects:

$$\alpha = r_0 . \left(\frac{\omega}{\upsilon}\right)^{\frac{1}{2}} \qquad (4)$$

where r_0 is the pipe radius and υ is the kinematic viscosity of the fluid.

Fig. 1 is a schematic diagram of the experimental setup. The working fluid used in the experiment is water. A pulsating flow can be obtained by superposition of a sinusoidal flow on a steady flow. A volumetric pump connected to a head tank of 300 litres provides the steady flow, as measured by an electromagnetic flow meter. The sinusoidal flow is generated by a Scotch-yoke mechanism. The dimensionless frequency α, which depends on the angular velocity of the pulsation ω, and also the velocity component ratio β, which depends on the piston stroke and the angular velocity ω, are controlled in the Scotch-yoke mechanism. The angular velocity of the pulsation ω is adjusted by a motor-speed reducer that controls crank velocity. A piston of 0.04 m diameter is connected to the crank by a metal stem; its stroke is controlled by the crank in 20 mm steps up to a maximum of 200 mm. The reliability of this Scotch-yoke mechanism in producing a sinusoidal flow has been verified in previous work [17] by LDV measurements of the axial velocity.

The steady and sinusoidal flows join each other at the inlet of a 2.5 m straight tube of circular cross section ($2r_0$= 40 mm). The sinusoidal flow, which is fully developed at the outlet of the straight tube, enters the test section. The test section is composed of six bends arranged in a chaotic configuration: the curvature plane of each bend makes a 90° angle with that of its neighbor. According to the numerical study of Jones et al. [22], a 90° angle is optimal for efficient stirring in steady alternating Dean flow. Each bend is a 90° curved pipe of circular cross section with cross-section diameter $2r_0$ = 40 mm and curvature radius r_c = 220 mm. The long straight tube and the bends are made of 5-mm thick Plexiglas.

A T-shaped Plexiglas flow divider was installed downstream of the curved pipe and PIV measurements were conducted at the pipe outlet (the flow divider eliminates light-refraction effects). The outer walls of the flow divider are flat and mirror polished. The cylindrical inner tubes have the same diameter as the bend cross-section (40 mm). The particles used for seeding are silver-coated hollow glass spheres (diameter 10 μm). The PIV camera is perpendicular to the illuminated outlet section of the curved pipe (Fig. 1) and acquires images through an optical window made of 3 mm thick float glass with a multilayer antireflection coating on both sides. A 7 Hz camera equipped with a Nikon lens (AF-Micro-NIKKOR 60mm) is used. A Nd YAG laser (50 mJ − 532 nm) provides a 2 mm thick laser sheet. Each image shows a 68.3-mm-square visualization window (2048×2048) centred on the flow field in the curved pipe cross section. Dynamic Studio software (version 2.30) is used for digital analysis of the pictures, particularly for the velocity computation. Adaptive correlation with interrogation zones of 64×64 pixels (50% area overlap) was used. The acquisition system is synchronized with the piston motion by an electronic power source that is controlled by a switching contact device. Each contact between the switch and the knob (which is on the crank periphery) sends a signal to the acquisition system. The acquisition then occurs after a delay time that is entered into the PIV control system and depends on the phase position ωt at which the velocity measurements are conducted. Four principal phase positions are studied here: ωt = 0°, 90°, 180° and 270°. Each velocity field is obtained by averaging at least 15 velocity fields measured for the same pulsating conditions at the same phase position.

3. Results and Discussions

3.1. Alternating Dean flow in steady regime

3.1.1. Topology of secondary flow

For Reynolds numbers Re_{st} = 420, 600, 800 and 1000, the velocity vector field of the secondary flow is measured in the steady state at the outlets of the first, second, third and sixth bends. Some additional measurements for Reynolds numbers Re_{st} = 300, 900, 1200 and 1500 were performed at the first bend outlet.

The secondary flow patterns at the bend outlets for Re_{st} = 420 and Re_{st} = 1000 are shown in Fig. 2 as representative examples. The x axis positive direction throughout the paper is toward the inner (convex) side of the bend, which is the closest wall to the curvature centre. For all Reynolds numbers, the secondary flow contains two counter-rotating cells whose centres are marked “+” in Fig. 2. Although the persistence of these two counter-rotating cells in all bends can be seen as a general similarity of the secondary flow structures for all Reynolds numbers studied, Fig. 2 shows that the symmetry (or asymmetry) of the flow structure and the positions of the cell centres depend strongly on Reynolds number and also

on bend number. To describe these dependences, the displacements of the cell centres were analyzed as detailed below.

Fig. 3 shows the definition of four parameters r_1, r_2, θ_1 and θ_2; r_1 and r_2 are the distances between the centre of each bend cross section and the cell centres close to the upper and lower walls, respectively. These distances are non-dimensionalized by the cross-section radius r_0. θ_1 and θ_2 are the angles between the vectors r_1 and r_2 and the x axis, respectively. The positive direction is taken in the trigonometric sense for θ_1 and in the antitrigonometric for θ_2 (Fig. 3).

For different bends, Fig. 4 and Fig. 5 show respectively the variations of $\frac{r_1}{r_0}$ and $\frac{r_2}{r_0}$ and of θ_1 and θ_2 with Reynolds number. The similarity between the curves of $\frac{r_1}{r_0}$ and $\frac{r_2}{r_0}$ (also between the curves of θ_1 and θ_2) in the first bend suggests the symmetry in the upper and lower cell positions with respect to the x axis. This symmetry is lost when the flow goes through the following bends, since the flow entry condition for the first bend is different from that for other bends: at the entrance to the first bend the flow is a fully developed Hagen–Poiseuille flow but that entering the next bends contains secondary circulations due to the previous bends.

Linear variation in the four parameters ($\frac{r_1}{r_0}$, $\frac{r_2}{r_0}$, θ_1 and θ_2) with Reynolds number can be observed in Fig. 4 and Fig. 5. Except for two points ($\frac{r_1}{r_0}$ at $Re_{st} = 420$ in the second and sixth bend), this linearity prevails in all the bends. Increasing the Reynolds number increases $\frac{r_1}{r_0}$ and $\frac{r_2}{r_0}$ and decreases θ_1 and θ_2 in the first bend. In other words, the higher the Reynolds number is, the farther are the cell centres (both the upper and the lower cells) from the cross-section centre, and the smaller are angles θ_1 and θ_2.

As all curves for the second, third and sixth bends are situated below those for the first bend (Fig. 4 and Fig. 5), it can be concluded that for known Reynolds number, the cells formed in the first bend are farther from the cross-section centre than those of the other bends. The angles θ_1 and θ_2 are also larger in the first bend than in the other bends.

In the range of all Reynolds numbers studied ($420 \leq Re_{st} \leq 1000$) in the third and sixth bends, and also when the Reynolds number is higher than 600 in the second bend, the upper cell moves away from the cross-section centre as the Reynolds number increases. In the second and third bend, θ_1 decreases with increasing Reynolds number; however, this angle is almost independent of Reynolds number in the sixth bend. Measurements of the lower cells formed after the first bend (Fig. 4 and Fig. 5) show that when the Reynolds number increases the lower cell is formed farther from the centre of the cross section in the second bend but closer to the cross-section centre in the third and sixth bends. In all bends, the angle θ_2 becomes smaller as the Reynolds number increases. Similarly to θ_1, the variations of θ_2 with Reynolds number are less significant in the sixth bend than in the other bends. The maximum and minimum distances between the upper cell centre and the centre of the section (and also

the maximum and minimum values of θ_1) were observed in the first and second bends, respectively. These (maximum and minimum) values for the lower cell occur in the first and sixth bend, respectively. According to Fig. 5, the angles θ_1 and θ_2 are always less than 90°; thus an important result is that the pair of cells in the secondary flow structure is maintained in the half-section close to the bend inner (convex) wall.

3.1.2. Mixing improvement: an advantageous mechanism with some drawbacks

Alternating Dean flow has shown many advantages in laminar mixing applications, especially for complex and very viscous fluids. The system is well adapted to continuous processes, and thanks to its geometry there is no need for external stirring: the Dean cells in the secondary flow play the role of internal agitators. Castelain et al. [6] have explained how the successive destruction and reformation of the secondary flow structures lead to the progressive destruction of the unmixed zones. The numerical study of Mokrani et al. [23] has also shown that the chaotic advection generated by spatial reorientation of the bends improves mixing quality.

The question arises whether these successive spatial reorientations of the bends also contribute to intensification of the axial vorticity and transverse strain rate. Vorticity and strain rate are used by Marble [24] to explain the mixing of two fluids. In fact, when the interface between two fluids of different properties is advected by the velocity field of a viscous flow, three distinct but interrelated effects contribute to mixing enhancement: engulfment, stretching and increase in the magnitude of species gradient. The vorticity causes engulfment of one fluid domain in another, after which the deformation of the interface continues by stretching. Finally, as the thickness of the fluid filaments at the interface decreases, the magnitude of the species gradient normal to the interface increases, thus intensifying molecular diffusion. On the basis of Marble's study [24], then, the evolution of strain rate and vorticity can be used as a criterion for mixing enhancement in a flow. Jarrahi et al. [21] used these two parameters to evaluate the role of secondary flow in transverse mixing. Thus if the axial vorticity and transverse strain rate are enhanced by successive spatial reorientations of the bends, it can be expected that alternating Dean flow in a *steady state* will enhance mixing in two different but simultaneous ways:

1. Mixing homogenization by progressive destruction of unmixed zones.

2. Intensification of axial vorticity and transverse strain rate leading to mixing enhancement.

The first aspect (mixing homogenization) has been the subject of all the studies cited above. The PIV measurements reported here also yield some new information on this issue: Fig. 6 shows the locus of the cell centres at the outlet from the first, second, third and sixth bends when the Reynolds numbers varies from 420 to 1000. The coordinates are nondimensionalized with the curved pipe cross-section radius:

$$\bar{x} = \frac{x}{r_0} \quad , \quad \bar{y} = \frac{y}{r_0} \tag{5}$$

In Fig. 6, the velocity vector planes of each bend outlet are rotated so that the positive direction of the *x* axis is always toward the convex wall of the bend; then the locus of the cell

centres is determined. Therefore, the 90° rotations in the cell positions, which are due to the orientation of the centrifugal force, are masked in Fig. 6.

Accordingly, although the cells centres move due to the successive reorientation of the curvature planes, they always remain inside a limited zone situated in the half-cross-section closer to the bend inner (convex) wall. For the Reynolds numbers studied here, this zone is distinguished by the rectangle in Fig. 6. The surface area of this zone is calculated and then nondimensionalized by the surface area of the curved pipe cross-section: the zone occupies only 9.2% of the bend cross-section. In other words, the movement of the cell centres is limited to less than 10 percent of the whole bend cross-section; the rest remains unoccupied and therefore inactive in mixing. The following sections analyse flow pulsation as a means of extending the zone visited by the cell centres in the bend cross section.

In discussing the second aspect of mixing enhancement, the evolutions of axial vorticity and transverse strain rate are used as a criterion. Axial vortices and transverse strain rate are defined as:

axial vorticity: $$\zeta(x,y) = \frac{\partial v}{\partial x} - \frac{\partial u}{\partial y} \qquad (6)$$

transverse strain rate: $$\varepsilon(x,y) = \frac{1}{2}\left(\frac{\partial v}{\partial x} + \frac{\partial u}{\partial y}\right) \qquad (7)$$

The reason for choosing these criteria has been discussed in previous work [8, 21, 24]. In fact, stretching and folding are the main contributions to mixing enhancement by strain rate and vorticity. The variations in cross-sectional averaged values of absolute axial vorticity ($|\zeta_S|$) and transverse strain rate ($|\varepsilon_S|$) are analysed. These values are obtained by averaging the absolute values of $\zeta(x, y)$ and $\varepsilon(x, y)$ at 1,200 points uniformly distributed in the tube cross section; the distance between two neighboring points is 1.02 mm.

Fig. 7 shows the variation in cross-sectional averaged values of absolute axial vorticity ($|\zeta_S|$) and transverse strain rate ($|\varepsilon_S|$) with the mean axial velocity (U_m) at the outlets of different bends. The subscript S denotes steady-state flow. Both axial vorticity and transverse strain rate increase linearly with increasing the flow velocity. In spite of this augmentation with the velocity, however, the axial vorticity and transverse strain rate decrease when the flow moves from one bend to the next, and this decrease becomes more significant at higher flow velocities ($U_m > 0.015$ m.s^{-1} i.e. $Re_{st} > 600$). Therefore, in steady state, the alternating Dean flow does not contribute to reinforcement of the axial vorticity and transverse strain rate fields; its only positive effect is homogenization. It will be shown that pulsation can relieve this shortcoming.

Before closing discussion of the steady regime, we point to the sample of velocity, axial vorticity and transverse strain rate fields in Fig. 8. Although the figure shows the distribution of these quantities at the exit from the first bend for $Re_{st} = 600$, the general structure of the secondary flow is similar for all Reynolds numbers in all bends: the secondary flow is always composed of two counter-rotating cells. This figure is discussed further in section 3.2.2, where the velocity, axial vorticity and transverse strain rate fields in *pulsating* flow are compared to the fields observed in *steady flow*.

3.2. Alternating Dean flow in pulsating regime

Jarrahi et al. [21] showed that some pulsating conditions, called “favorable conditions”, enhance transverse mixing in a 90° bend compared to the steady flow. The superposition of these favorable pulsating conditions ($\beta \geq 2$ and $\alpha \leq 15$) on Dean flow results in higher values of vorticity and strain rate than in the steady state. Furthermore, the secondary flow structures formed in pulsating regimes are more complex than those in the steady regime. These observations support the idea that pulsation can also intensify mixing in alternating Dean flow. In this section, the effects of different pulsating conditions (summarized in table 1) on transverse mixing in the alternating Dean flow are studied in order to determine favorable conditions for such intensification.

3.2.1. Mixing enhancement: intensification of vorticity and strain rate

Having explained the roles of vorticity and strain rate on mixing intensification, Jarrahi et al. [21] introduced two parameters ($\overline{A}_\zeta$ and $\overline{A}_\varepsilon$) to assess global transverse mixing during a complete oscillation period. The same criteria are used here to evaluate transverse mixing in the pulsating alternating Dean flow. The integral of the cross-sectional averaged value of absolute vorticity curve during an oscillation period in a *pulsatile flow* is called $A_P(\zeta)$ and the same integral in the corresponding *steady flow* is called $A_S(\zeta)$; the dimensionless parameter $\overline{A}_\zeta$ can be defined as the ratio of $A_P(\zeta)$ to $A_S(\zeta)$:

$$\overline{A}(\zeta) = \frac{A_p(\zeta)}{A_S(\zeta)} = \frac{\frac{1}{2\pi}\int_0^{2\pi} |\zeta_P|}{|\zeta_S|} \tag{8}$$

Similarly, the dimensionless parameter for transverse strain rate, $\overline{A}_\varepsilon$, is defined as

$$\overline{A}(\varepsilon) = \frac{A_p(\varepsilon)}{A_S(\varepsilon)} = \frac{\frac{1}{2\pi}\int_0^{2\pi} |\varepsilon_P|}{|\varepsilon_S|} \tag{9}$$

The subscripts S and P refer to the steady and pulsating regimes.

The values of $\overline{A}(\zeta)$ and $\overline{A}(\varepsilon)$ for all the pulsating conditions are presented as histograms in Fig. 9 and Fig. 10, respectively, where a group of four columns is associated with each pulsating condition ($\{Re_{st}, \beta$ and $\alpha\}$). Each column in a group represents the value of $\overline{A}(\zeta)$ (or $\overline{A}(\varepsilon)$) calculated at the outlet of one of the bends (first, second, third or sixth). The value 1 for $\overline{A}(\zeta)$ and $\overline{A}(\varepsilon)$ indicates the *steady flow*, i.e. with no pulsation.

A pulsation condition is favourable for transverse mixing if all columns of the associated group are greater than 1 for both $\overline{A}(\zeta)$ and $\overline{A}(\varepsilon)$. In such condition, a pulsating alternating Dean flow is more efficient for mixing than a steady Dean flow. In Fig. 9 and Fig. 10, the

groups associated with favourable pulsating conditions are marked by ☑. It can be seen that for all pulsating conditions, even if not "favourable," the transverse mixing is intensified in the first and second bends compared to the steady flow. However, the pulsation is not always advantageous: in some pulsating conditions, the values for $\overline{A}(\zeta)$ and $\overline{A}(\varepsilon)$ are below 1 in the third and sixth bends. This unfavourable effect of some pulsating conditions becomes more significant in the last (sixth) bend. For example, according to the vorticity criterion $\overline{A}(\zeta)$, the condition $\{Re_{st} = 420, \beta = 1, \alpha = 14{,}51\}$ intensifies transverse mixing compared to the steady flow in the first and second bends by up to 27% and 1%, respectively. However, the same condition decreases transverse mixing in the third and sixth bends by up to 18% and 27%, respectively. Therefore, a "favourable pulsating condition" also depends on the number of bends in the mixer structure. If the mixer has only two bends, the pulsation is always interesting in the range of conditions studied here, i.e. $\{420 \leq Re_{st} \leq 1000, 1 \leq \beta \leq 4, 8.37 \leq \alpha \leq 24.5\}$. The greater the number of bends, the fewer favourable pulsating conditions exist.

The favorable pulsating conditions distinguished in Fig. 9 and Fig. 10 are for a mixer composed of six bends. The common parameter among these favourable conditions is Womersley number α below 15.4. In other words, the high-frequency pulsations ($\alpha > 15.4$) are not advantageous for mixing even if the velocity component ratios β are high: using a high-frequency pulsation, even with the highest β value, decreases $\overline{A}(\zeta)$ and $\overline{A}(\varepsilon)$. This effect is more significant in the last bend: see the columns for the condition $\{Re_{st} = 420, \beta = 4, \alpha = 20.53\}$). In fact, when the Womersley number is high due to the high pulsating frequency, the viscous effects are confined to a thin layer near the bend wall, while the main part of the core flow in the transverse section is almost inviscid. Therefore, the velocity gradients in the middle of the pipe cross section remain small and the fluid particles passing through this region do not experience strong stretching. In contrast to this unfavourable effect of high Womersley number (α), the results show that high values of the velocity component ratio β are of interest for transverse mixing enhancement, especially when $\alpha \leq 15.4$.

Table 2 summarises the minimum and maximum transverse mixing increases in different bends for the favourable pulsating conditions identified here. The increase is calculated by comparison with the steady-state values at the same bend. It can be concluded that imposing a pulsation on the steady flow in a six-bend chaotic mixer can intensify transverse mixing from 20% to 430% on average. Therefore, a pulsating alternating Dean flow improves mixing in laminar regime.

3.2.2. Improving mixing by enlarging cell movement zones

The advantages of a steady alternating Dean flow for mixing are related to the successive destruction and reformation of the Dean cells. The periodic destruction of the KAM (unmixed) zones located around the cell centres (elliptic points) leads to more efficient mixing than in a helically coiled (regular) Dean flow. However, this advantage is limited because the movement of the cells occurs only in limited zones close to the inner (convex) wall that cover less than 10% of the curved tube cross-section. Therefore, any mechanism that makes the cell movement zones spread over more of the cross-section should improve mixing in alternating Dean flow.

Previous work [21] showed the complexity of the movement of the cell centres during an oscillation period in a pulsatile flow passing through a 90° curved pipe. Here we investigate whether this pulsation-generated complexity persists in the other bends of the alternating Dean flow. Complexities that expand the movement zones of the cells over those in steady regime should contribute to mixing improvement in alternating Dean flow.

Measurements of the secondary flow at the outlets of the second, third and sixth bends confirm that, for the same pulsating conditions, the flow structures are even more complex than those observed in a single bend (see Fig. 11). As a representative example, the secondary flow structures for a favourable pulsating condition {Re_{st} = 600, β = 2, α =10.26} are shown in Fig. 12-15; note that the oscillation ($\omega.t$) phase at the first bend inlet is taken as reference in determining the phase of the pulsating flow. At the same oscillation phase, the general structure of the secondary flow is similar for the second, third and sixth bends. However, it is slightly different for the first bend (Fig. 11), especially when the sinusoidal component of the axial velocity is zero, in other words when $\omega.t$ = 0° or $\omega.t$ =180°. The following paragraphs give more details on these structures.

At $\omega.t$ = 0°, where the pulsating velocity, $U_P(t)$, is equal to the mean steady flow, U_{st}, a siphon structure is formed in the second, third and sixth bends (Fig. 12) composed of one counter-clockwise rotating cell. High-vorticity regions are situated at the position where the cell is formed, but the high-strain-rate regions are located outside and around the cell. The secondary flow structure at $\omega.t$ = 0° is different in the first bend, where a no-cell structure appears (Fig. 11). However, the same figure confirms that a siphon structure is also generated in the first bend but at $\omega.t$ = 315°, i.e. 45° before the following bends.

When the flow rate is maximum ($\omega.t$ = 90°), the secondary flow in the second, third and sixth bends is composed of two counter-rotating cells close to the convex wall of the bend (Fig. 13). This structure, called deformed Dean circulation (DDC), is similar to that observed in the first bend (Fig. 11). The cell that is closer to the upper wall of the bend cross-section rotates clockwise and the other cell rotates counter-clockwise. The regions in which the cells appear have the highest values of vorticity, but high-strain-rate regions are also situated in the neighbourhood.

The most complex structure in the second, third and sixth bends is observed at $\omega.t$ = 180° where the pulsating velocity, $U_P(t)$, and the mean steady flow, U_{st}, become equal again, but this time in the middle of the deceleration zone of the oscillation curve. This four-cell structure is shown in Fig. 14. In the upper (lower) half of the cross section, the cell close to the inner (outer) wall rotates clockwise and the other cell, close to the outer (inner) wall, rotates counter-clockwise. This relatively large number of cells results in a distribution of velocity gradients in the flow cros-section that is more efficient for mixing, as shown by the vorticity and strain-rate fields in Fig. 14. According to Jarrahi et al. [21], the secondary flow at $\omega.t$ = 180° in the first curved pipe resembles the two-bean structure consisting of two counter-rotating cells (Fig. 11). This structure, called "circulation intermediate between Dean and Lyne," can be considered the primitive form of the four-cell structure observed here in the second, third and sixth bends.

Fig. 15 shows the secondary flow structure in the second, third and sixth bends when the flow rate is minimum ($\omega.t$ = 270°). A backward axial flow occurs in this oscillation phase. The secondary flow has an asymmetric structure composed of two counter-rotating cells that is similar to the structure observed in the first bend (Fig. 11).

A qualitative comparison of different secondary flow structures, vorticity and strain rate fields observed in *steady* (Fig. 8) and *pulsating* alternating Dean flow (Fig. 11-15) confirms the advantages of pulsation in generating complex flow structures, extending the cell movement zones and also distributing strong velocity gradients. Furthermore, in the pulsatile secondary flow, the fluid particles remain in the flow transverse section for a longer time than in a steady flow before they follow the axial flow [25]. The complexity of secondary flow structures implies also reduction in axial dispersion, which is advantageous for mixing. However, this should be confirmed by residence-time distribution method (RTD) [2,3] to understand the effects of each pulsating condition (Re, α, β) on axial dispersion. Since the flow is time-dependent, a numerical simulation is more adapted to the RTD method.

The locus of the centres of secondary flow cells was studied in order to evaluate the effect of pulsation on the size of the zones in which the cells move. The dimensionless positions of the cell centres at the outlets of the first, second, third and sixth bends are shown in Fig. 16 for *steady flow* with Re_{st} = 600 and for *pulsatile flow* with favourable condition {Re_{st} = 600, β = 2, α =10,26}. The zone associated with the movement of the cells in the *steady* alternating Dean flow is confined to a narrow rectangle close to the bend convex wall, while this zone in pulsating alternating Dean flow covers a wide, almost square rectangle. The surface area of the rectangle in the steady flow covers only 5.5% of the curved pipe cross section, while that of the pulsating flow expands to 50.5% of the cross section. In other words, the superposition of a favourable pulsating condition on the steady flow in an alternating Dean geometry (chaotic mixer) enlarges the movement zone of the centres of internal stirrers (cells) up to nine times over the steady flow. Furthermore, the number of cells increases. These observations confirm the mixing advantages of pulsation in an alternating Dean flow.

4. Conclusions

The secondary flow velocity fields in steady and pulsating alternating Dean flows are investigated by PIV measurements. Some secondary flow structures not observed before are found. Furthermore, tracing the evolution of axial vorticity and transverse strain rate as well as analysis of the Dean cell movements allowed assessment of the mixing in the flow.The experimental results reported here show that pulsation enhances mixing in an alternating Dean flow (chaotic geometry).

In the *steady* case, it was observed that the secondary flow structure is always composed of two counter-rotating cells close to the convex wall in all bends. However, the symmetry (or asymmetry) of the flow structure and the positions of the cell centres depends on the number of bends and also the Reynolds number. Moreover, study of the transverse mixing in steady alternating Dean flow showed that the values of axial vorticity and transverse strain rate decrease with successive changes in the orientation of the curvature planes. The only positive effect on transverse mixing in steady flow of alternating the orientation of the curvature planes is related to the successive destruction of the unmixed zones around the cell centres, a mechanism contributing to mixing homogenization. However, the cells move through less than 10% of the curved pipe cross-section in the steady flow.

The *pulsating* alternating Dean flow showed that the transverse mixing is enhanced between 20% to 430% by increasing β when $\alpha \leq 15.4$. Furthermore, when a favourable pulsating condition is applied, the locus of the cell centres occupies a zone that is nine times

larger than the steady-state occupied zone. The advantages of pulsation in a chaotic mixer operating in the laminar regime are thus clear.

Energy consumption of the mixer should also be considered for estimating the global efficiency of the mixer. Both “energy used for generating pulsations” and “energy dissipated in the mixer” should be taken into account. The former can be estimated based on kinetic energy of the piston that generates pulsations; the latter is related to the pressure drop in the mixer. However, the design of our experimental setup does not allow us to measure the pressure drop in pulsating conditions. In other words, we cannot capture the effects of each pulsating condition on pressure drop through the mixer. Ignoring the pressure drop, the discussion can be limited to the energy used for generating sinusoidal component of the flow, i.e. $U_{\sin}(t) = U_{ms}.\beta.\sin(\omega.t)$, during one period. This energy is proportional to the integral of $U_{\sin}^2$ in a period, which is equal to $\frac{\upsilon.\pi}{4}(\frac{\mathrm{Re}_{st}.\beta}{\alpha})^2$. Therefore, the energy used for generating sinusoidal component of the flow varies with Re_{st}^2 , β^2 and $(1/\ \alpha)^2$. Between favorable pulsating conditions that were identified for a given Re_{st}, the condition with a lower β and higher α is more interesting.

It should be pointed out that the flow under consideration is three-dimensional; there are thus three principal directions of strain rate (and vorticity). In this study, the axial velocity could not be measured due to the form of the curved pipe; therefore, the results are limited to the axial vorticity and transverse strain rate. A follow-up study, probably numerical, is required to determine three-dimensional velocity field and also the principal axes of strain rate tensor. Then, the angle between intermaterial area and the principal axes of strain rate tensor, which is an insightful parameter to analyze mixing enhancement, can be determined for each pulsating condition.

NOMENCLATURE

r_o Pipe cross-sectional radius

r_c Curvature radius

u Velocity in x direction

v Velocity in y direction

Re Reynolds number, $\mathrm{Re} = \dfrac{U_m(2r_0)}{\upsilon}$

Greek symbols

α Womersley number, $r_o(\omega/\upsilon)^{1/2}$

β Velocity component ratio

υ Kinematic viscosity

η Curvature ratio of curved pipe , r_o/r_c

ω Angular frequency

$\zeta(x,y)$ Axial vorticity at position (x,y) in the curved pipe cross-section: $\dfrac{\partial v}{\partial x} - \dfrac{\partial u}{\partial y}$

$|\zeta_P|$ Cross-sectional average value of absolute vorticity in a pulsatile flow

$|\zeta_S|$ Cross-sectional average value of absolute vorticity in a steady flow

$\varepsilon(x,y)$ Transverse strain rate at position (x,y) in the curved pipe cross-section: $\dfrac{1}{2}(\dfrac{\partial v}{\partial x} + \dfrac{\partial u}{\partial y})$

$|\varepsilon_P|$ Cross-sectional average value of absolute transverse strain rate in a pulsatile flow

$|\varepsilon_S|$ Cross-sectional average value of absolute transverse strain rate in a steady flow

Subscripts

P Pulsating flow
S Steady flow

References

[1] H. Aref, Stirring by chaotic advection, J. Fluid Mech., 143 (1984) 1-21.

[2] C. Castelain, A. Mokrani, P. Legentilhomme, H. Peerhossaini, Residence time distribution in twisted pipe flows: helically coiled system and chaotic system, Exp. Fluids 22 (1997) 359-368.

[3] C. Habchi, T. Lemenand, D. Della Valle, H. Peerhossaini, Liquid/liquid dispersion in a chaotic advection flow, Int. J. Multiphase Flows, 35 (2010), 485-497.

[4] N. Achrya, M. Sen, H.C. Chang, Heat transfer enhancement in coiled tubes by chaotic mixing, Int. J. Heat Mass Transf. 35 (1992) 2475-2489.

[5] N. Achrya, M. Sen, H. C. Chang, Thermal entrance length and Nusselt numbers in coiled tubes, Int. J. Heat Mass Transf. 37 (1994) 336-340.

[6] C. Chagny, C. Castelain, H. Peerhossaini, Chaotic heat transfer for heat exchanger design and comparison with a regular regime for a large range of Reynolds numbers, Appl. Therm. Eng. 20 (2000), 1615-1648.

[7] C. Castelain, A. Mokrani, Y. Le Guer, H. Peerhossaini, Experimental study of chaotic advection regime in a twisted duct flow, Eur. J. Mech. B-Fluid 20 (2001) 205-232.

[8] T. Lemenand, H. Peerhossaini, A thermal model for prediction of the Nusselt number in a pipe with chaotic flow, Appl. Therm. Eng., 21 (2002), 1717-1730.

[9] T.J. Pedley, The fluid mechanics of large blood vessels. Cambridge University Press, 1980.

[10] L.J. Chang, J.M. Tarbell, Numerical simulation of fully developed sinusoidal and pulsatile (physiological) flow in curved tubes, J. Fluid Mech. 161 (1985), 175-198.

[11] M. Siouffi, V. Deplano, R. Pelissier, Experimental analysis of unsteady flows in stenosis, J. Biomech. 31 (1988), 11-19.

[12] L. Zabielski, A.J. Mestel, Unsteady blood flow in a helically symmetric pipe, J Fluid Mech. 370 (1998), 321-345.

[13] V. Deplano, M. Siouffi, Experimental and numerical study of pulsatile flows through stenosis: wall shear stress analysis, J. Appl. Biomech. 32 (1999), 1081-1090.

[14] O. Boiron, V. Deplano, R. Pelissier, Experimental and numerical studies on the starting effect on the secondary flow in a bend, J. Fluid Mech. 574 (2007) 109-129.

[15] J.H. Siggers, S.L. Waters, Unsteady flows in pipes with finite curvature, J. Fluid Mech. 600 (2008), 133-165.

[16] H.A. Simon, M.H. Chang, J.F.C. Chow, Heat transfer in curved tubes with pulsatile, fully developed, laminar flows, ASME J. Heat Transf. 99 (1977), 590-595.

[17] B. Timité, M. Jarrahi, C. Castelain, H. Peerhossaini, Pulsating flow for mixing intensification in a twisted curved pipe, ASME J. Fluid Eng. 131 (2009), 121104.1-121104.10.

[18] W.H. Lyne, Unsteady viscous flow in a curved pipe, J. Fluid Mech. 45 (1970), 13-31.

[19] M. Sumida, K. Sudo, H. Wada, Pulsating flow in a curved pipe (secondary flow), JSME Int. J. 32 (1989), 523-531.

[20] K. Sudo, M. Sumida, R. Yamane, Secondary motion of fully developed oscillatory flow in curved pipe, J. Fluid Mech. 237 (1992), 189-208.

[21] M. Jarrahi, C. Castelain, H. Peerhossaini, Secondary flow patterns and mixing in laminar pulsating flow through a curved pipe, Exp. Fluids 50 (2011), 1539-1558.

[22] S. Jones, O.M. Thomas, H. Aref, Chaotic advection by laminar flow in twisted pipe, J. Fluid Mech. 209 (1989), 335-357.

[23] A. Mokrani, C. Castelain, H. Peerhossaini, Mesure du comportement chaotique des trajectories produites dans un écoulement de Dean alterné en regime laminaire, Rev. Gen. Therm., 37 (1998), 459-474.

[24] F.E. Marble, Growth of a diffusion flame in the field of a vortex, Recent Advances in the Aerospace Sciences, Plenum Publishing, New York, 1985.

[25] M. K. Sharp, R. D. Kamm, A. H. Shapiro, E. Kimmel, G. E. Karnidakis, Dispersion in a curved tube during oscillatory flow, J. Fluid Mech., 223 (1991) 537–563.

List of tables

Figure Captions:

Fig. 1. Schematic of experimental setup.

Fig 2. Structures of secondary flow in steady alternating Dean flow for Re_{st} = 420 and 1000.

Fig. 3. Measured parameters to locate centres of secondary flow cells.

Fig. 4. Variations in $\frac{r_1}{r_0}$ and $\frac{r_2}{r_0}$ with Reynolds number in different bends.

Fig. 5. Variations in θ_1 and θ_2 with Reynolds number in different bends.

Fig. 6. Locus of the cell centres at the bend outlets in steady alternating Dean flow with Reynolds number varying between 420 and 1000.

Fig. 7. Variations in axial cross-sectional average values of absolute axial vorticity ($|\zeta_S|$) and transverse strain rate ($|\varepsilon_S|$) with Reynolds number at the bend outlets.

Fig. 8. Representative fields of secondary flow velocity, axial vorticity and transverse strain rate at the bend outlets in steady alternating Dean flow.

Fig. 9. $\overline{A_\zeta}$ for $\{420 \leq Re_{st} \leq 1000,\ 1 \leq \beta \leq 4,\ 8.37 \leq \alpha \leq 24.5\}$ in pulsating alternating Dean flow.

Fig. 10. $\overline{A_\varepsilon}$ for $\{420 \leq Re_{st} \leq 1000,\ 1 \leq \beta \leq 4,\ 8.37 \leq \alpha \leq 24.5\}$ in pulsating alternating Dean flow.

Fig. 11. Secondary flow variation in an oscillation period, Re_{st}=600, β=2, α=10.26. Velocity values at lower left are the highest velocities, shown as red vectors in the velocity field, for each case. The lowest velocities are the blue vectors, between 0 mm/s and 1 mm/s (Jarrahi, Castelain & Peerhossaini 2011).

Fig. 12. Representative fields of secondary flow velocity, axial vorticity and transverse strain rate at the outlets of the second, third and sixth bends when ω.t = 0° in pulsating alternating Dean flow.

Fig. 13. Representative fields of secondary flow velocity, axial vorticity and transverse strain rate at the outlets of the second, third and sixth bends when ω.t = 90° in pulsating alternating Dean flow.

Fig. 14. Representative fields of secondary flow velocity, axial vorticity and transverse strain rate at the outlets of the second, third and sixth bends when ω.t = 180° in the pulsating alternating Dean flow.

Fig. 15. Representative fields of secondary flow velocity, axial vorticity and transverse strain rate at the outlets of the second, third and sixth bends when $\omega.t = 270°$ in the pulsating alternating Dean flow.

Fig. 16. Locus of the cell centres formed at the outlets of the bends in steady (Re_{st}=600) and pulsating (Re_{st}=600, β=2, α=10.26) alternating Dean flow.

	$Re_{st} = 420$	$Re_{st} = 600$	$Re_{st} = 800$	$Re_{st} = 1000$
β=1	α = 8.37 α =10.26 α =14.51	α = 8.37 α =10.26 α =12.14 α =17.77	α = 12.14 α =14.51 α =20.53	α = 10.26 α =11.24 α =15.4
β=2	α = 10.26 α =14.51 α =20.53	α =10.26 α =14.51 α =17.77 α =24.5		
β=3	α= 10.26 α =14.51 α =17.77			
β=4	α= 14.51 α =20.53			

Table 1: Pulsating conditions studied

	Vorticity criterion		Strain rate criterion	
	Min	**Max**	**Min**	**Max**
Bend 1	15%	400%	22%	375%
Bend 2	36%	527%	35%	536%
Bend 3	12%	477%	23%	450%
Bend 6	3%	348%	13%	308%

Table 2: Minimum and maximum increase in transverse mixing in different bends

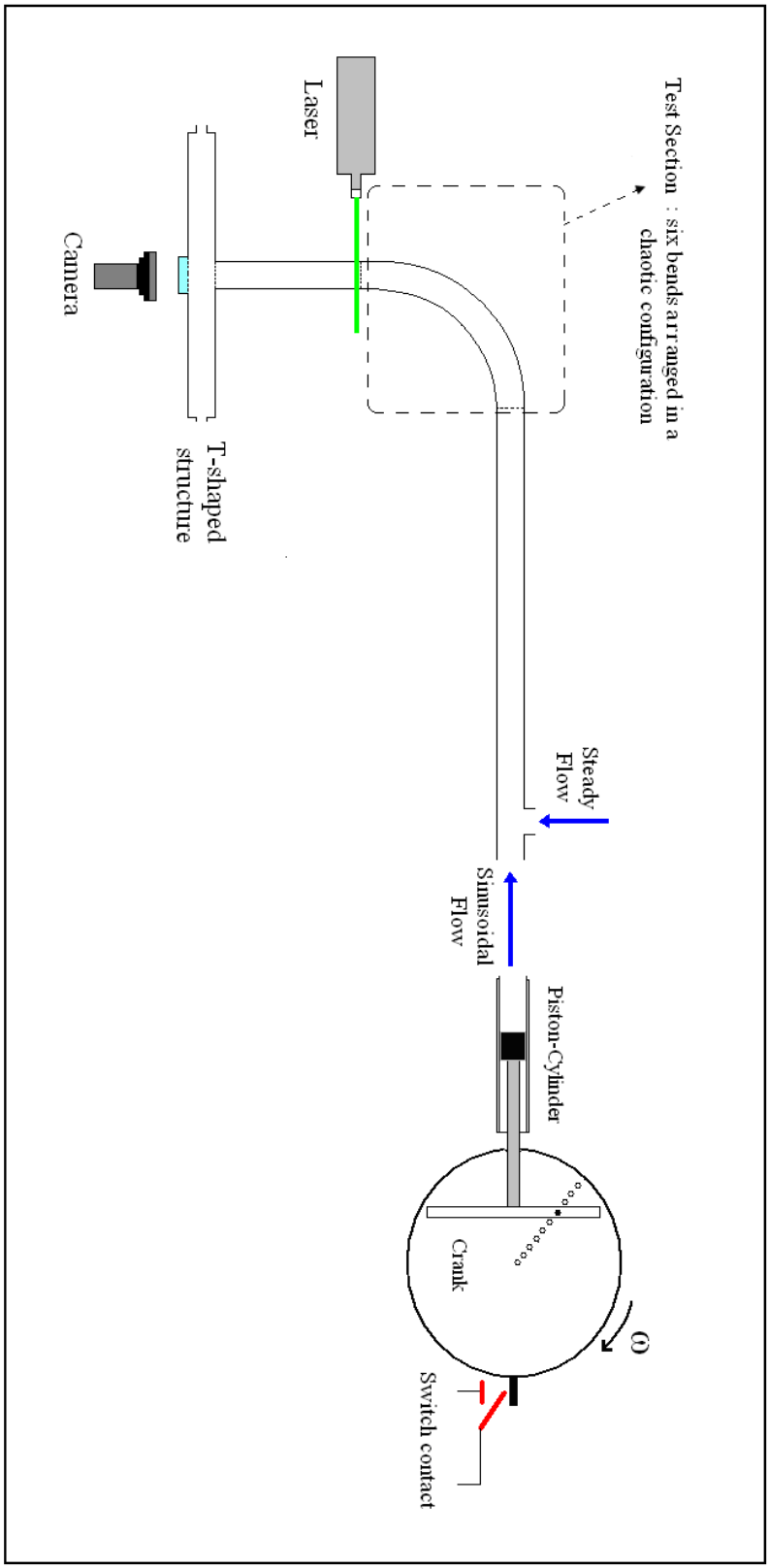

Fig. 1. Schematic of experimental setup

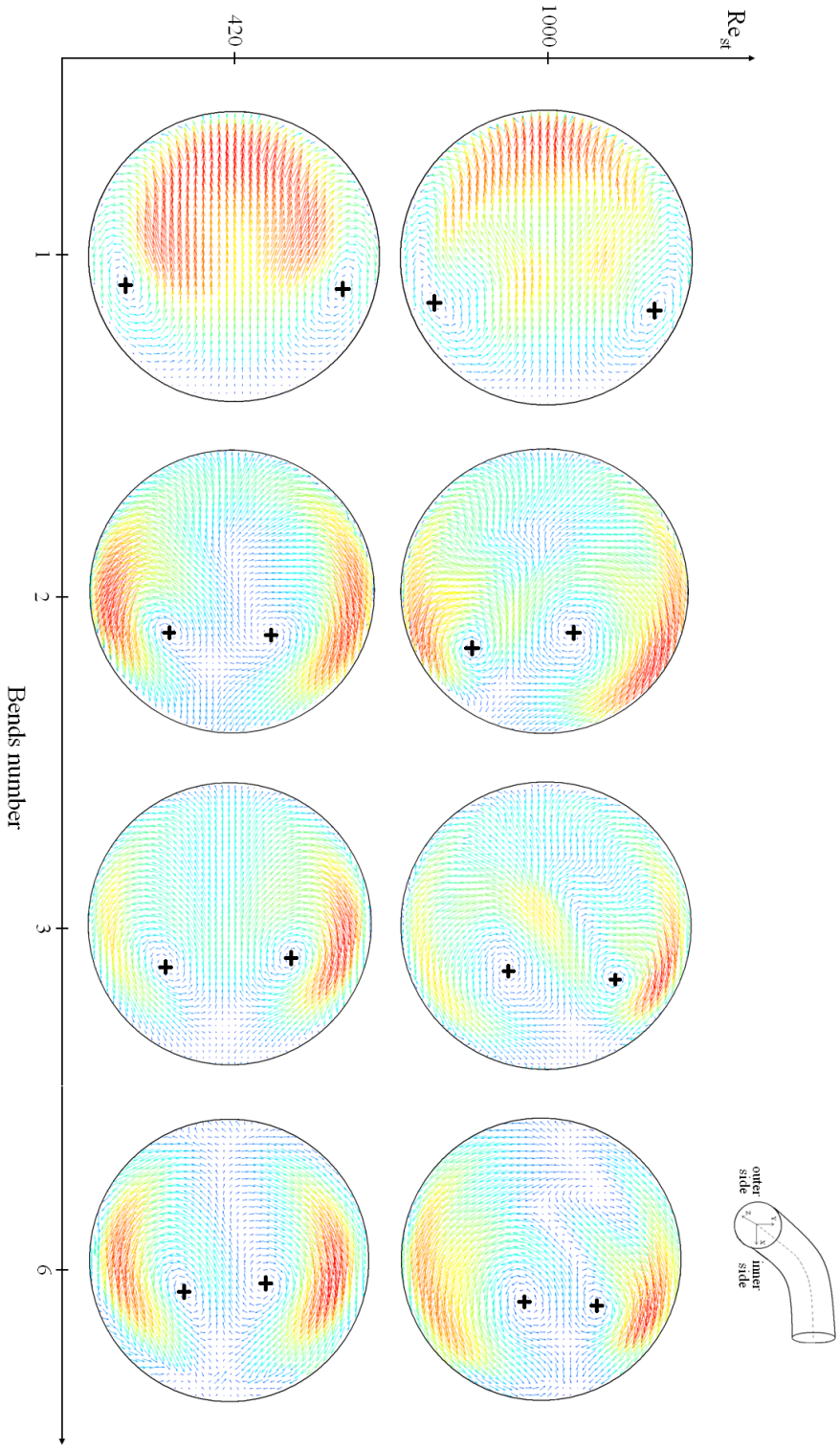

Fig. 2. Structures of secondary flow in steady alternating Dean flow for $Re_{st} = 420$ and 1000

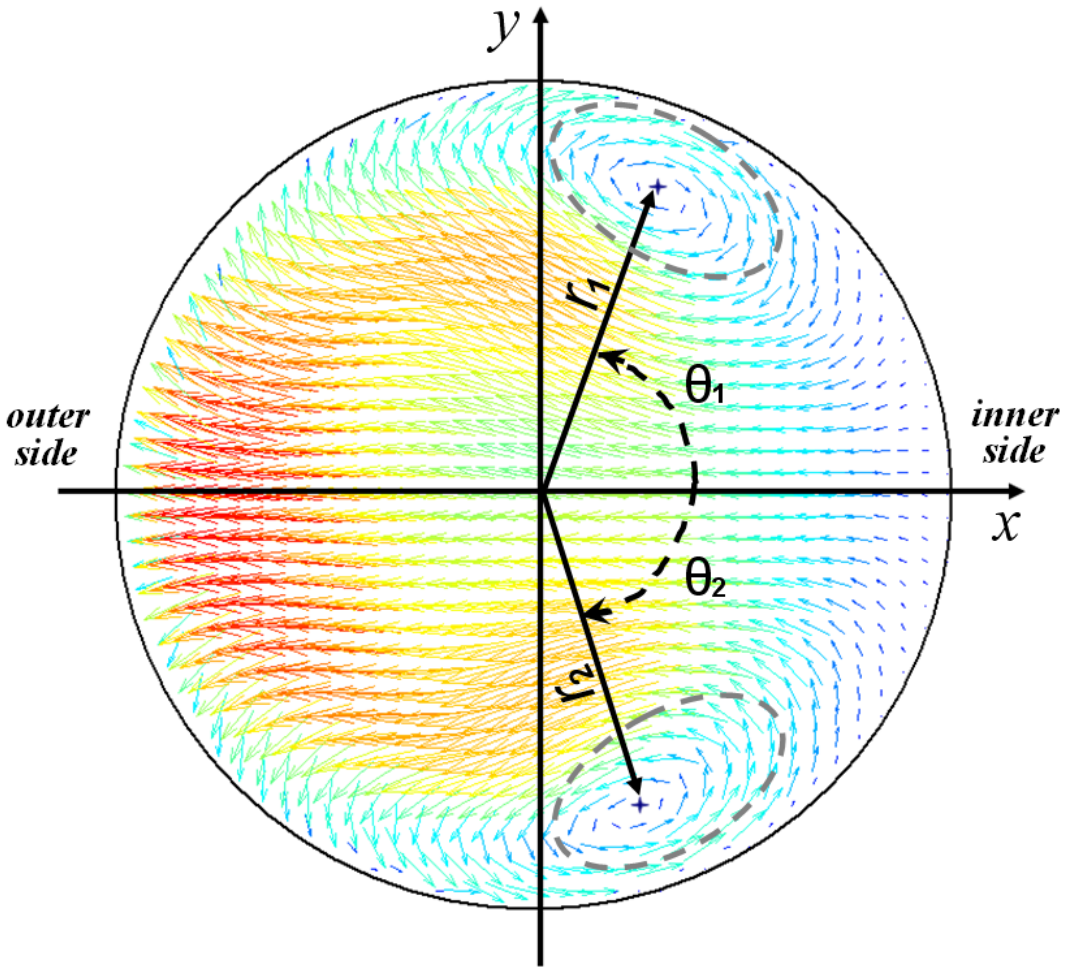

Fig. 3. Measured parameters to locate centres of secondary flow cells

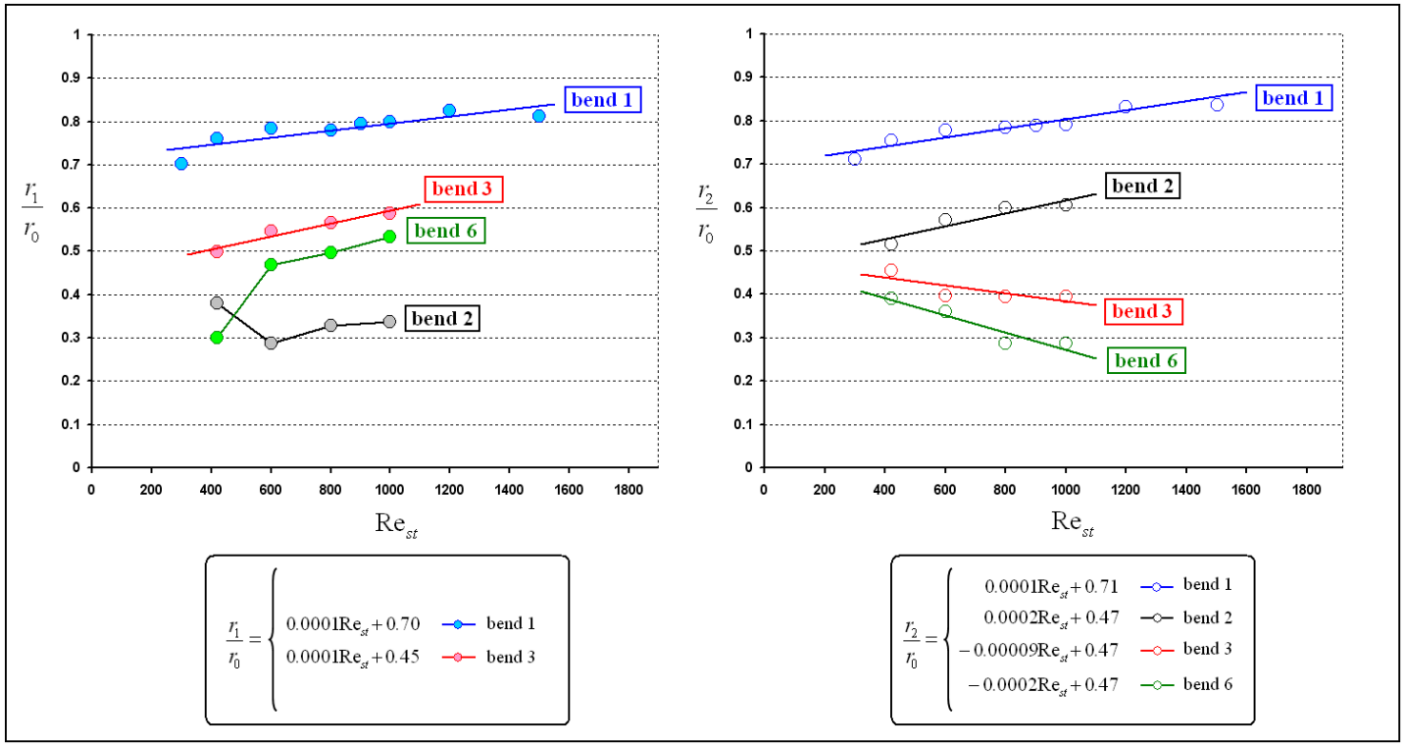

Fig. 4. Variations in $\frac{r_1}{r_0}$ and $\frac{r_2}{r_0}$ with Reynolds number in different bends

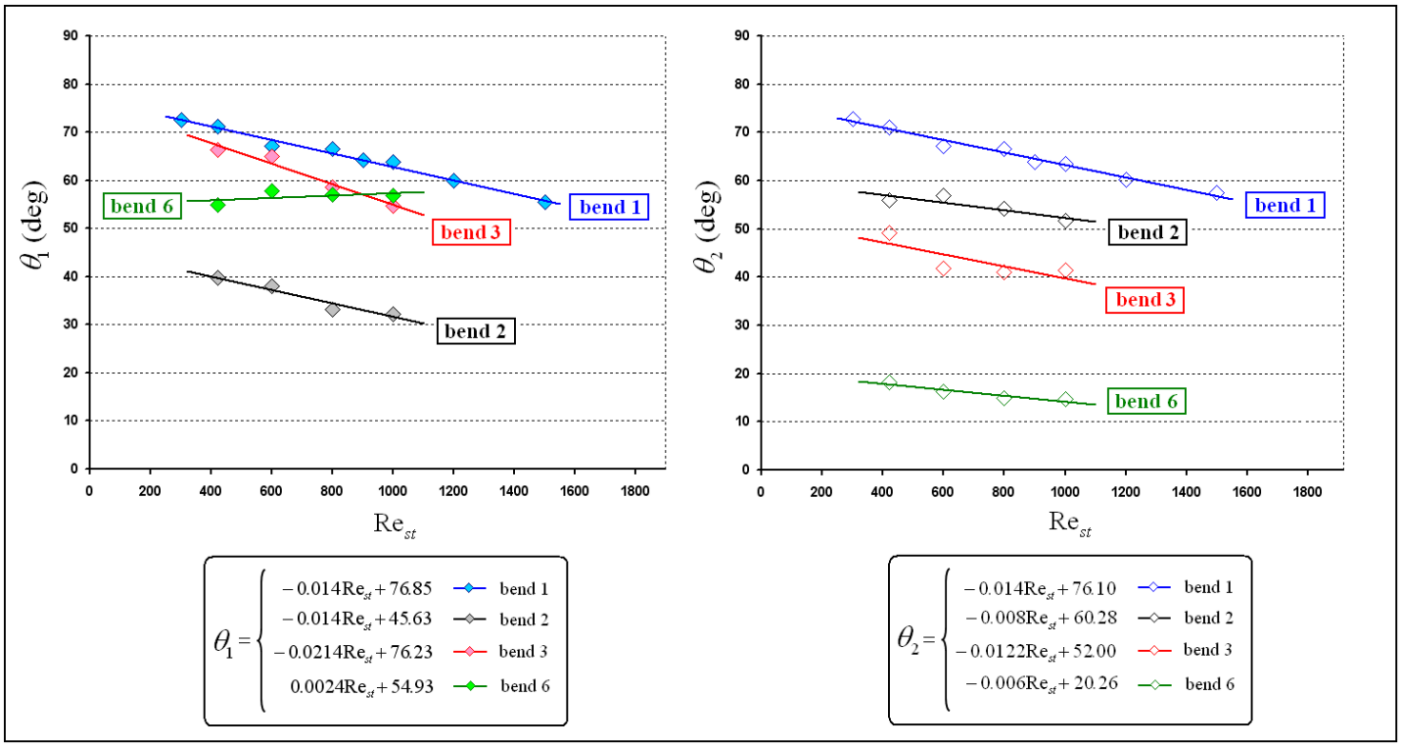

Fig. 5. Variations in θ_1 and θ_2 with Reynolds number in different bends

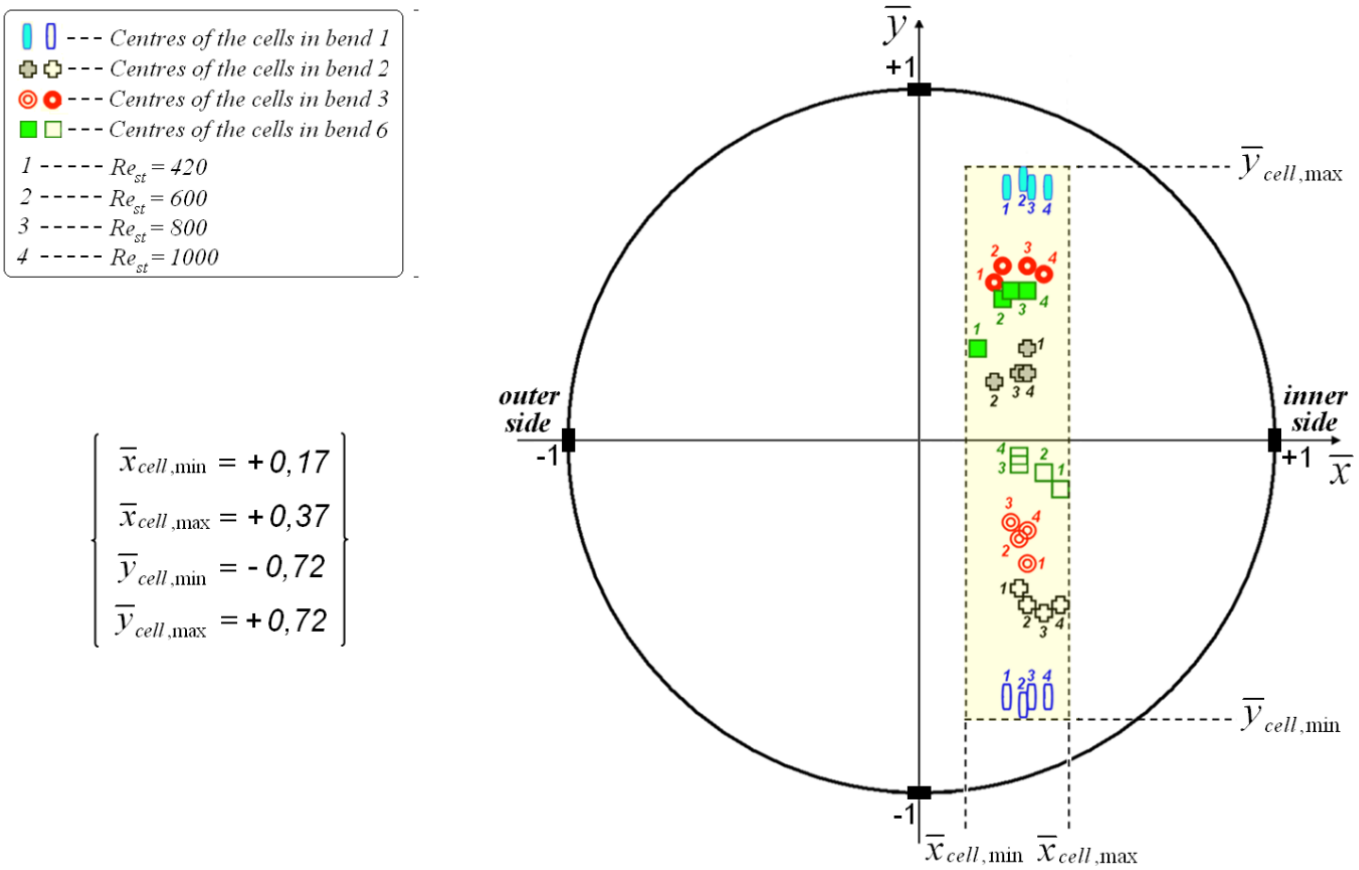

Fig. 6. Locus of the cell centres at the bend outlets in steady alternating Dean flow with Reynolds number varying between 420 and 1000

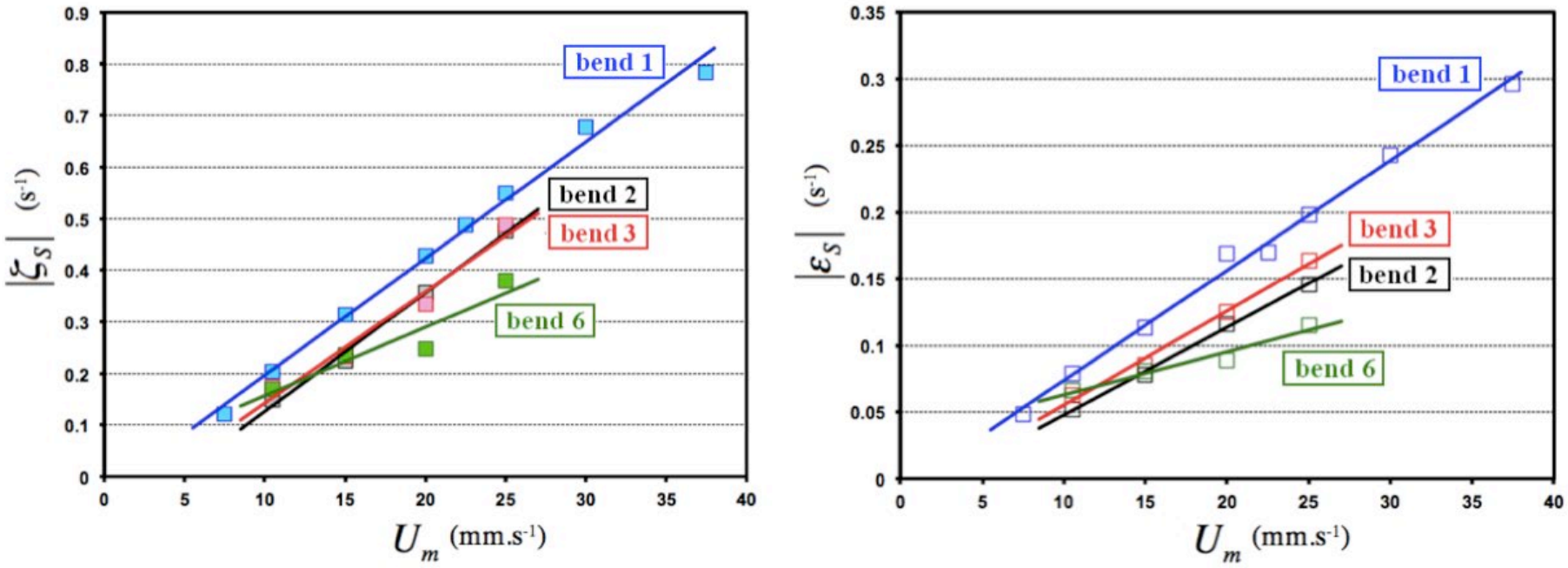

Fig. 7. Variations in axial cross-sectional average values of absolute axial vorticity ($|\zeta_S|$) and transverse strain rate ($|\varepsilon_S|$) with the mean velocity of steady flow at the bend outlets

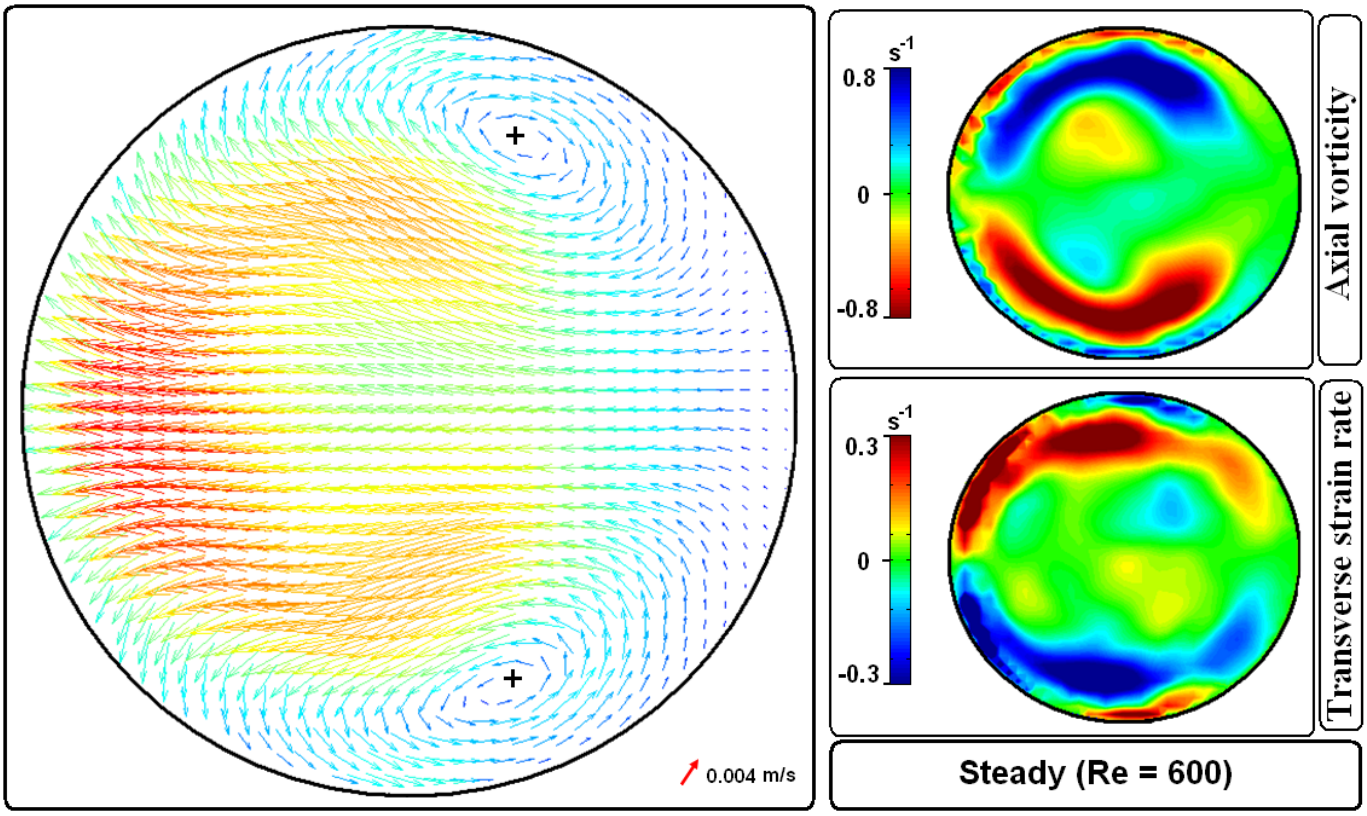

Fig. 8. Representative fields of secondary flow velocity, axial vorticity and transverse strain rate at the bend outlets in steady alternating Dean flow

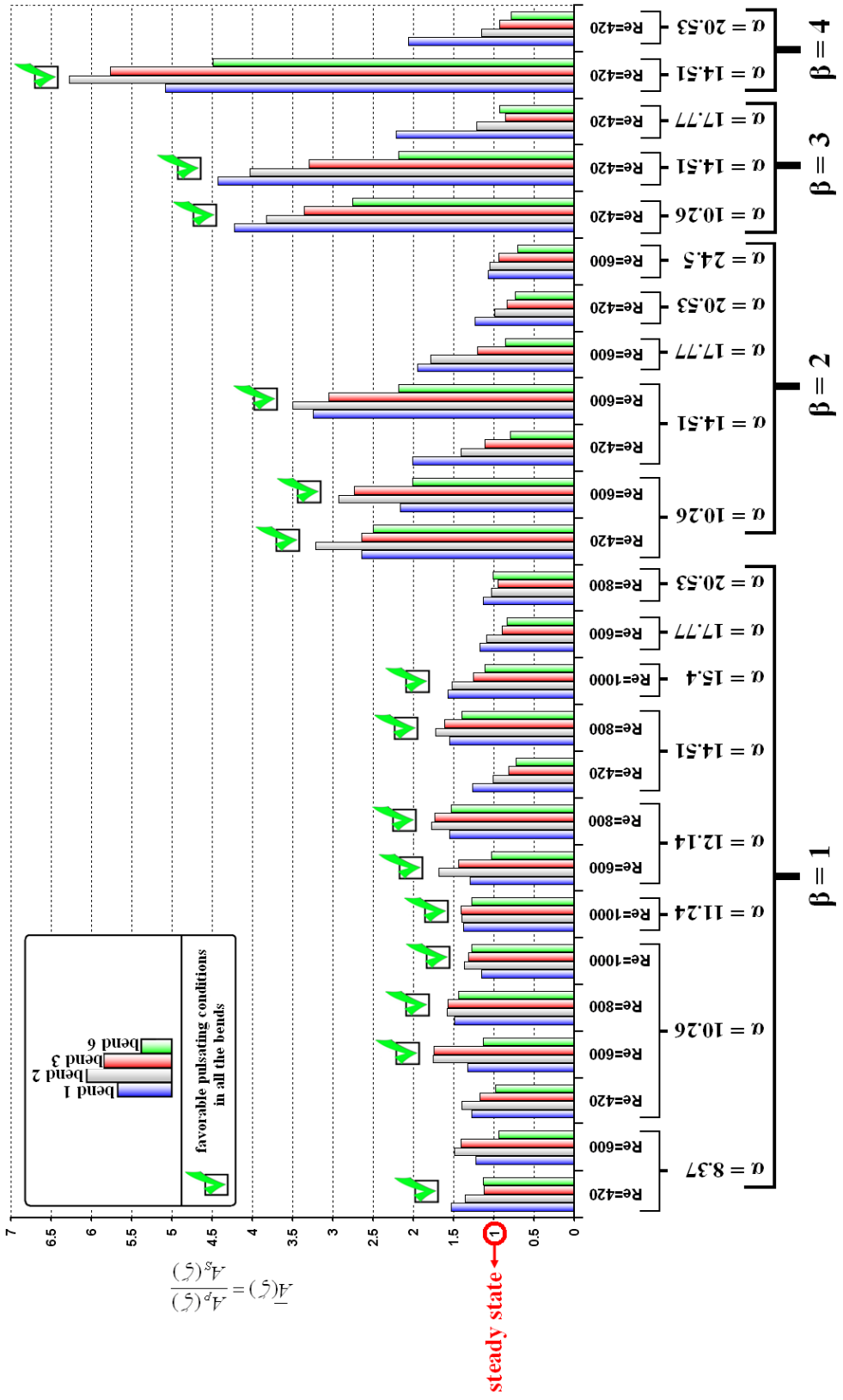

Fig. 9. $\overline{A_\zeta}$ for {420≤Rest≤1000, 1≤β≤4, 8.37≤α≤24.5} in pulsating alternating Dean flow

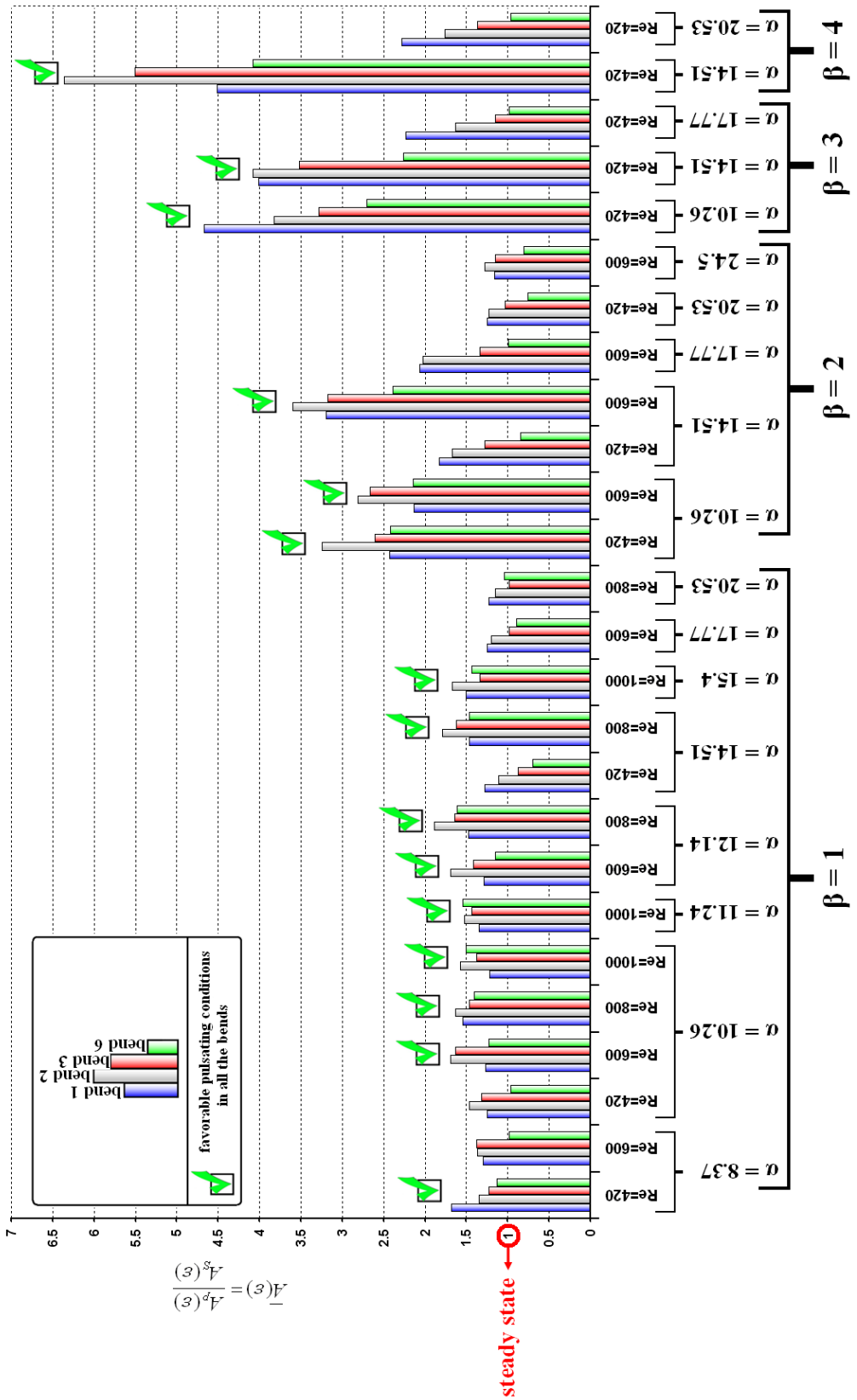

Fig. 10. $\overline{A_\varepsilon}$ for {420≤Rest≤1000, 1≤β≤4, 8.37≤α≤24.5} in pulsating alternating Dean flow.

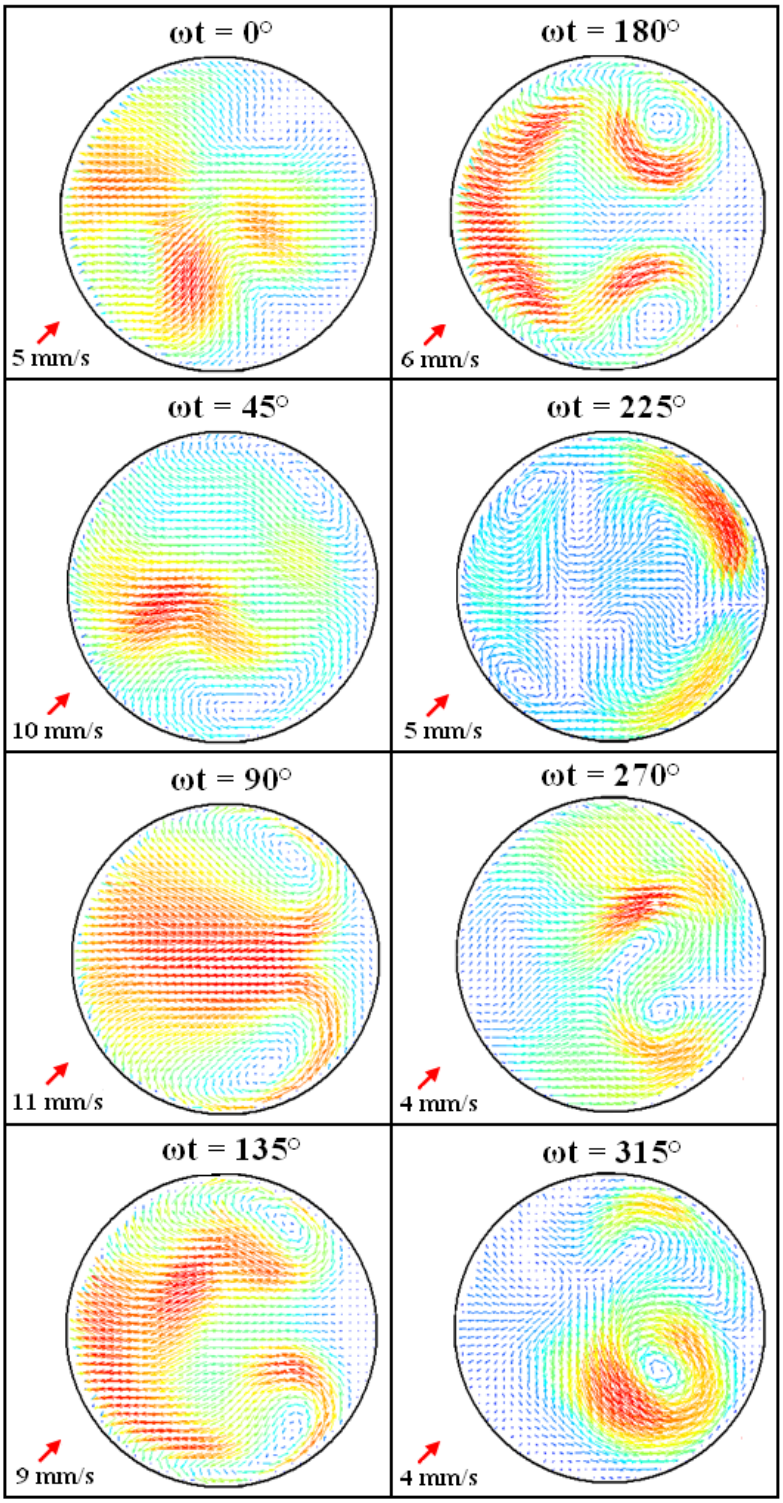

Fig. 11. Secondary flow variation in an oscillation period, Re_{st}=600, β=2, α=10.26. Velocity values at lower left are the highest velocities, shown as red vectors in the velocity field, for each case. The lowest velocities are the blue vectors, between 0 mm/s and 1 mm/s (Jarrahi, Castelain & Peerhossaini 2011).

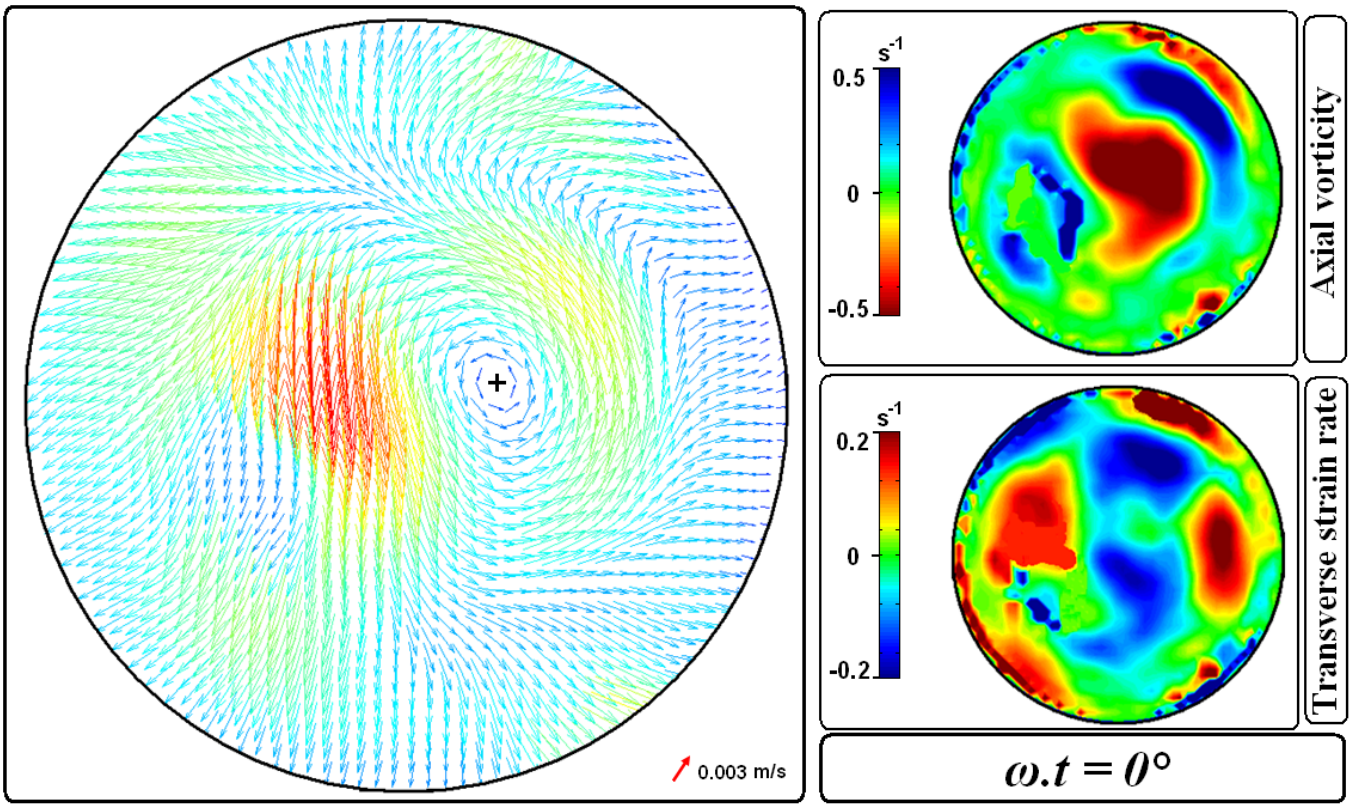

Fig. 12. Representative fields of secondary flow velocity, axial vorticity and transverse strain rate at the outlets of the second, third and sixth bends when ω.t = 0° in pulsating alternating Dean flow

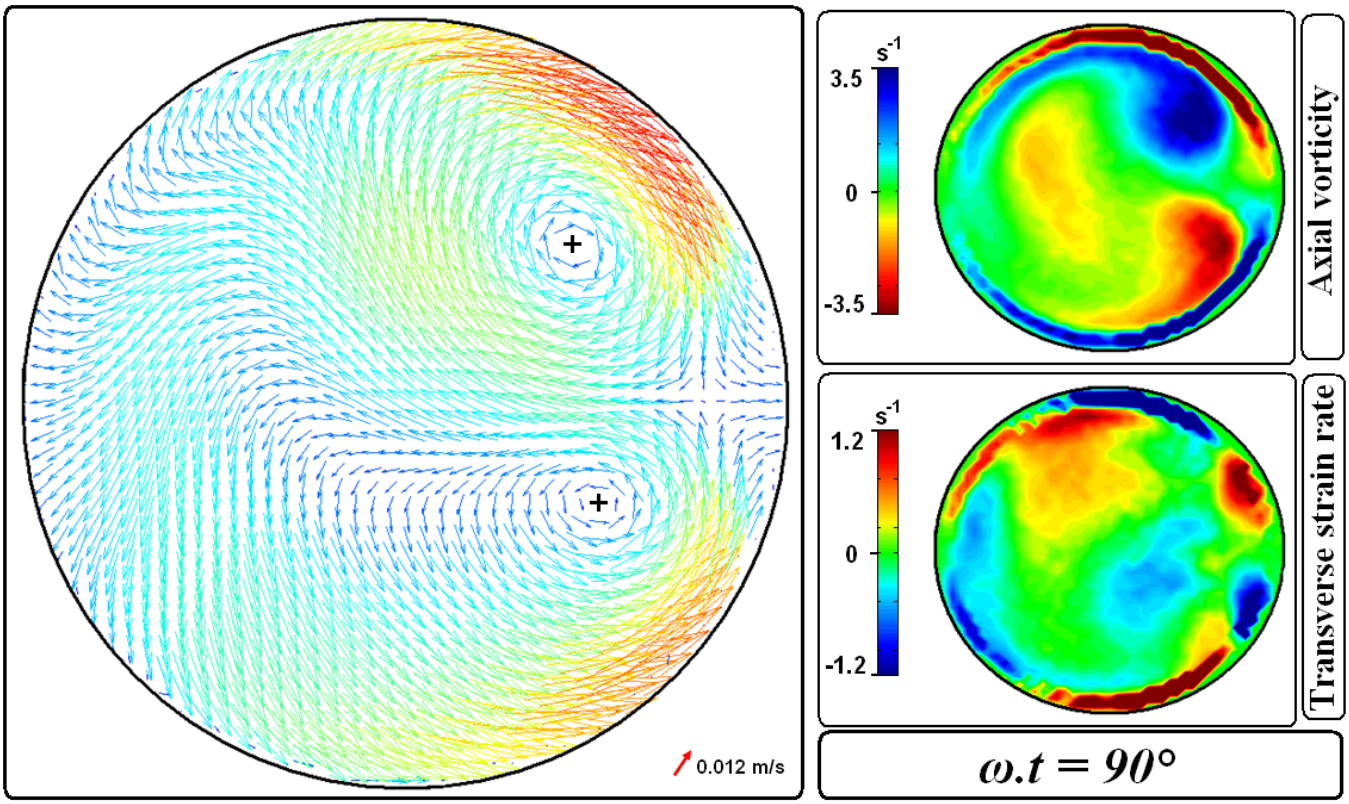

Fig. 13. Representative fields of secondary flow velocity, axial vorticity and transverse strain rate at the outlets of the second, third and sixth bends when ω.t = 90° in pulsating alternating Dean flow

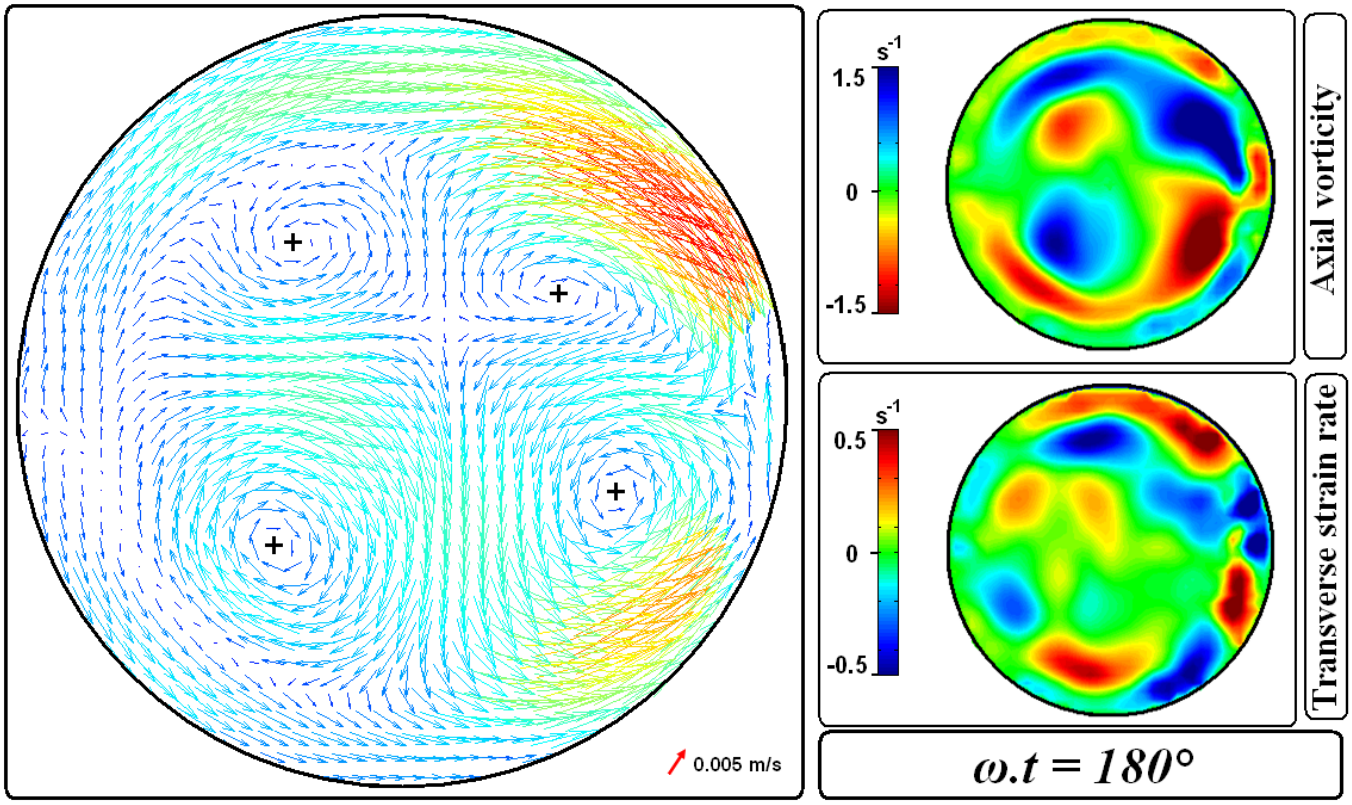

Fig. 14. Representative fields of secondary flow velocity, axial vorticity and transverse strain rate at the outlets of the second, third and sixth bends when ω.t = 180° in the pulsating alternating Dean flow

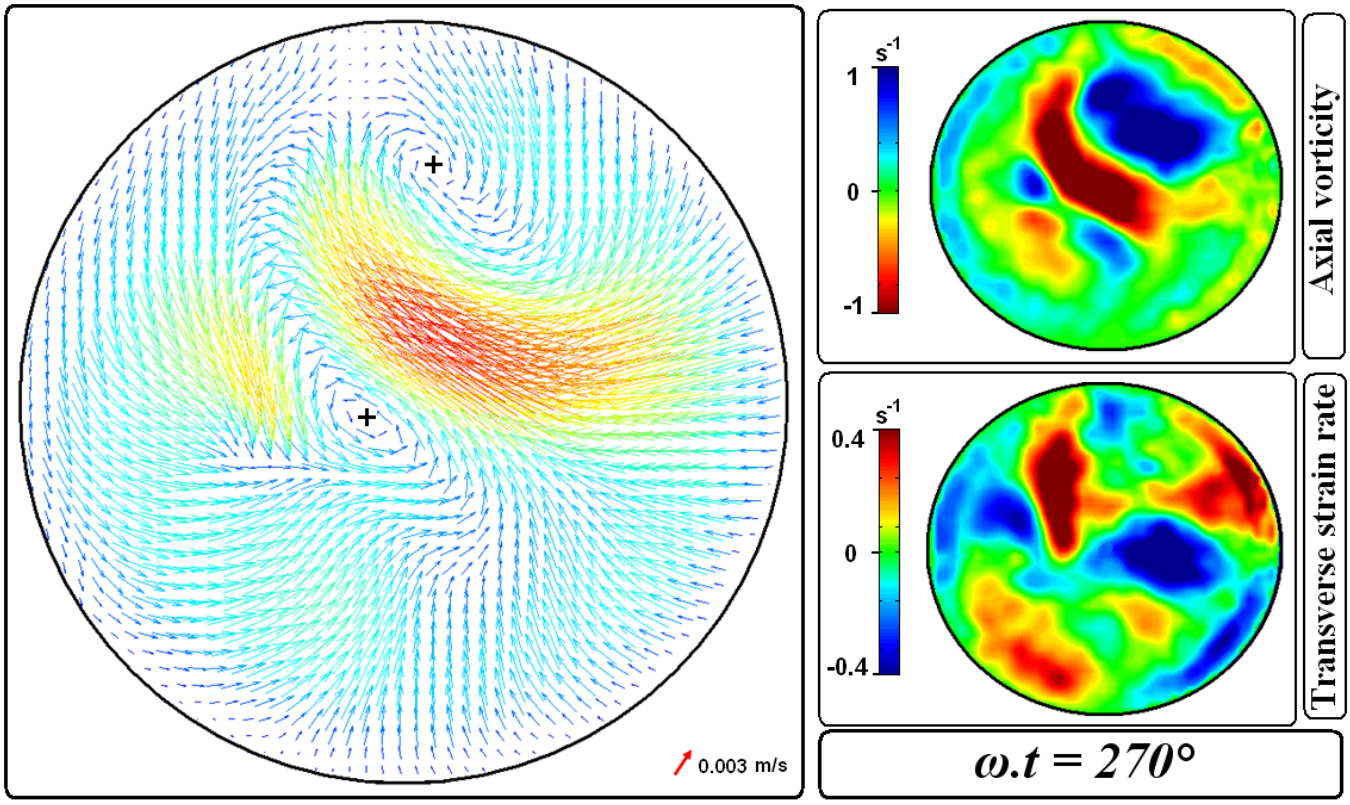

Fig. 15. Representative fields of secondary flow velocity, axial vorticity and transverse strain rate at the outlets of the second, third and sixth bends when ω.t = 270° in the pulsating alternating Dean flow

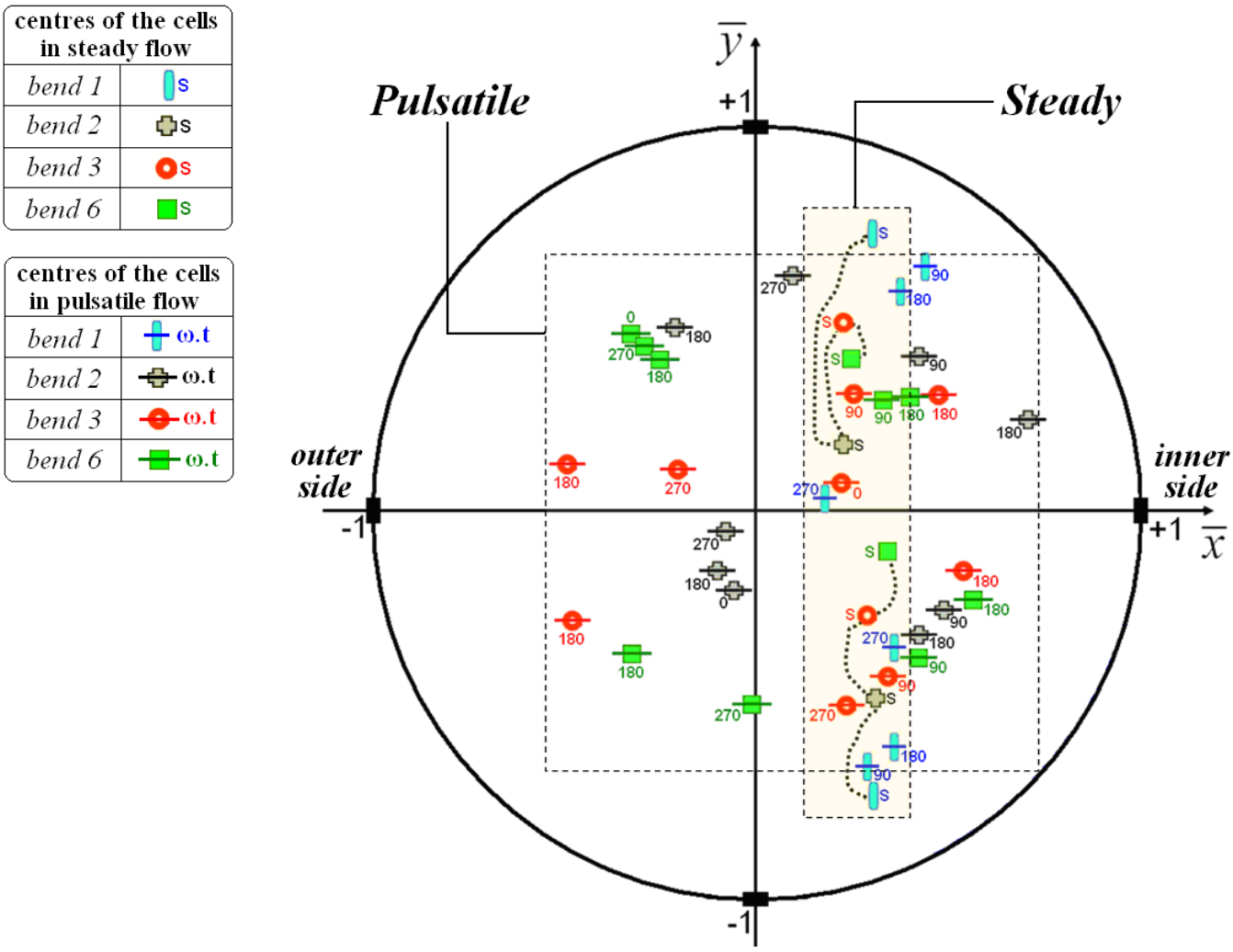

Fig. 16. Locus of the cell centres formed at the outlets of the bends in steady (Re_{st}=600) and pulsating (Re_{st}=600, β=2, α=10.26) alternating Dean flow